Magnetoelastic coupling and the magnetization plateau in $Ba_3CoSb_2O_9$

M. Li,[1,2] A. Zelenskiy,[1] J. A. Quilliam,[2] Z. L. Dun,[3] H. D. Zhou,[3] M. L. Plumer,[1] and G. Quirion[1,2]
[1]*Department of Physics and Physical Oceanography, Memorial University, St. John's, Newfoundland, Canada A1B 3X7*
[2]*Institut Quantique and Département de Physique, Université de Sherbrooke, Sherbrooke, Québec, Canada J1K 2R1*
[3]*Department of Physics and Astronomy, University of Tennessee, Knoxville, Tennessee 37996-1200, USA*

(Received 21 September 2018; revised manuscript received 7 January 2019; published 6 March 2019)

High-precision ultrasonic measurements are used to study magnetoelastic coupling as a function of the in-plane magnetic field orientation in the spin-1/2 triangular lattice antiferromagnet $Ba_3CoSb_2O_9$. The relevance of this coupling in stabilizing the 1/3 magnetization plateau is explored. The analysis indicates that, while the magnetoelastic coupling in $Ba_3CoSb_2O_9$ is large in comparison to other triangular lattice antiferromagnets, the strength of this coupling is still too small to fully account for the magnetization plateau width in $Ba_3CoSb_2O_9$. Spin fluctuations are therefore the dominant mechanism inducing and stabilizing the magnetization plateau. Our results also show that the amplitude of the spin fluctuations suddenly drop as the V phase is induced at higher field.

DOI: 10.1103/PhysRevB.99.094408

I. INTRODUCTION

Geometrically frustrated triangular lattice antiferromagnets (TLAFs) have been widely studied in recent decades, as they show an impressive variety of exotic magnetic states [1–3]. The discovery of a magnetization plateau in a number of TLAFs with easy-plane anisotropy makes these systems even more fascinating [4–8]. The magnetization plateau is observed at a value of 1/3 of the magnetization saturation (m_s) for a magnetic field applied in the triangular plane [4–11]. This plateau is known to be associated with the collinear up-up-down (uud) state with two spins parallel to the field while the third one is antiparallel. The magnetic field–temperature phase diagrams of TLAFs have also been the object of multiple theoretical and numerical studies [12–17]. For example, the magnetic phase diagram by M. V. Gvozdikova *et al.* [12], determined from Monte Carlo simulations using a classical Heisenberg model for two-dimensional (2D) TLAFs, is shown in Fig. 1(a). According to these simulations and other numerical works [13,15–17], the anticipated spin configurations correspond to the 120° order at zero field, Y state, uud state, and V state, as illustrated in Fig. 1(a). As shown in Fig. 1(b), these predictions compare well with recent experimental results obtained for the spin-1/2 easy-plane quasi-2D TLAF $Ba_3CoSb_2O_9$ where $T_N = 3.8$ K [18]. While this simple classical model accounts well for the observed phase sequence as a function of the field, as well as a magnetization plateau associated with the collinear uud state for $T > 0$ K [12], it fails considerably at $T = 0$ K where the width of the magnetization plateau collapses, in contradiction with the experimental observations (Fig. 1(b) [18]).

Considering that thermal fluctuations generally favor collinear states [12,16], it has been proposed and shown that quantum fluctuations can be the mechanism for lifting the classical degeneracy in favor of the uud state at $T = 0$ K [14,16,19]. This is also supported by real-space perturbation theory [20,21] which shows that the effects of spin fluctuations in TLAFs can be taken into account by considering a classical model with a biquadratic exchange coupling term between nearest neighboring magnetic ions. The 2D Heisenberg model, with biquadratic exchange coupling, can then be expressed as

$$E = J \sum_{i \neq j} \mathbf{s}_i \cdot \mathbf{s}_j - \gamma \sum_{i \neq j} (\mathbf{s}_i \cdot \mathbf{s}_j)^2 - \mathbf{H} \cdot \sum_i \mathbf{s}_i. \qquad (1)$$

where $J > 0$ and γ are the nearest-neighbor exchange and the biquadratic exchange constants, respectively. In this effective classical model, it is then straightforward to show that the magnetization plateau width is directly determined by the strength of the biquadratic coefficient γ. For the quasi-2D TLAF $Ba_3CoSb_2O_9$, using the experimental values $J/k_B = 18.5$ K, $g = 3.84$ [8], $|\mathbf{s}_i| = 1/2$ [7], and setting $\gamma/J = 0.2$, we obtain the model magnetization at $T = 0$ K shown in Fig. 2 (blue dashed line) which agrees well with the magnetization curve measured at $T = 1.3$ K (black continuous line) [8]. Furthermore, the spin configurations derived from Eq. (1) at $T = 0$ K are consistent with those obtained from Monte Carlo simulations [12] (see Fig. 1).

The microscopic origin of the biquadratic exchange coupling term [Eq. (1)] can also be associated with the spin-lattice coupling (magnetoelastic coupling) [22–25], in addition to quantum and thermal fluctuations. This scenario is especially pertinent in the case of $Ba_3CoSb_2O_9$, since large sound velocity variations ($\Delta v/v \simeq 7\%$) are observed as a function of the magnetic field, reflecting strong magnetoelastic coupling [18]. In the present work, we therefore study the relevance of the magnetoelastic coupling relative to quantum fluctuations in stabilizing the magnetization plateau in this archetype spin-1/2 quantum TLAF material [7,8,26,27]. Our goal is achieved using an experimental approach based on ultrasound velocity measurements [28]. It consists in measuring the relative velocity variation of an acoustic mode at constant temperatures and fields as the in-plane field direction is changed relative to

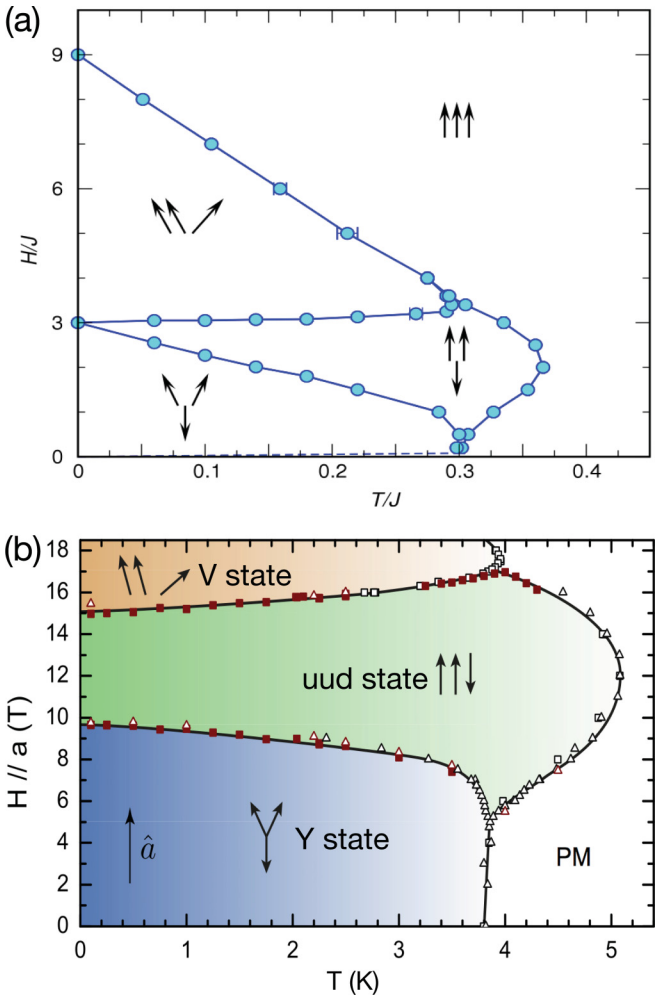

FIG. 1. (a) Reproduction of the H-T phase diagram of TLAFs determined using Monte Carlo simulations by Gvozdikova *et al.* [12]. (b) Experimental H-T phase diagram of $Ba_3CoSb_2O_9$ obtained by ultrasonic measurements [18] for the field parallel to the basal plane.

the a axis. The measured field angular dependence, $\Delta v(\phi)/v$, is then analyzed within the framework of a mean-field model in order to determine the magnetoelastic coupling constants which account for the lattice distortions. Based on the field dependence of the magnetoelastic coupling determined at 2.5 K, the strength of the magnetoelastic coupling is too small to account for the magnetization plateau in $Ba_3CoSb_2O_9$. The results rather show the the field dependence of the velocity is dominated by spin fluctuations which increase as a function of the field. The results also indicate that the amplitude of these spin fluctuations suddenly drops as the V phase is stabilized.

The remainder of the paper is organized as follows. We briefly describe the experimental methods in Sec. II, while the experimental results are presented and described in Sec. III. In order to analyze the field angular dependence of relative velocity variation, $\Delta v(\phi)/v$, measured at constant temperatures and fields, a mean-field model which explicitly takes into account the magnetoelastic coupling for a hexagonal lattice structure is used. This approach, presented in Sec. IV, conveniently leads to analytical solutions for the field angular dependence $\Delta v(\phi)/v$ and the elastic deformations (strains).

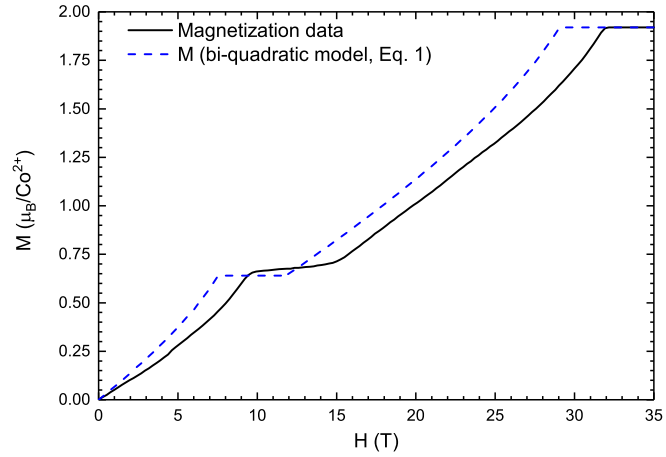

FIG. 2. Black continuous line representing the experimental field dependence of magnetization of $Ba_3CoSb_2O_9$ measured at 1.3 K for the $\mathbf{H} \parallel ab$ plane, obtained by Susuki *et al.* [8], is compared to numerical calculation based on the biquadratic model, Eq. (1) (blue dashed line).

These solutions are used to fit the experimental data in order to determine the strength of magnetoelastic coupling in the paramagnetic state (Sec. V A) and the ordered states (Sec. V B). This allows us to identify the contributions associated with the uniform magnetization m relative to the antiferromagnetic spin modulation S. Finally, Sec. VI contains a summary and conclusion regarding the most significant findings and observations.

II. EXPERIMENT

Sound velocity measurements were carried out using longitudinal acoustic modes generated and detected with two 30 MHz $LiNbO_3$ transducers mounted on opposite polished faces (transmission configuration). For this investigation, the longitudinal modes propagating along the a axis of a single crystal with a length of 2.57 mm were used to determine the ultrasound velocity $v_{L[100]}$. The relative velocity variation $\Delta v(\phi)/v$, measured at constant temperatures and magnetic fields using a pulsed acoustic interferometer operating around 100 MHz for higher resolution [29], was then recorded as the $Ba_3CoSb_2O_9$ crystal was rotated about c axis by an angle ϕ, changing the field direction in the ab plane. Here, $\phi = 0^\circ$ corresponds to the magnetic field parallel to the direction of propagation of the acoustic mode $v_{L[100]}$ (a axis).

III. EXPERIM ENTAL RESULTS

In Fig. 3, we present the field angular (ϕ) dependence of the relative variation of sound velocity ($\Delta v_{L[100]}/v$) measured at different field values: in the paramagnetic state at $T = 10$ K and in the ordered states at $T = 2.5$ K. In the paramagnetic state, a well defined angular period of 180° is observed with a maximum at $\phi \sim 0$ (corresponding to $\mathbf{H} \parallel a$ axis) and a minimum close to $\phi = -90^\circ$. In the Y state, additional extrema emerge around $\phi = -40^\circ$ and -130° while the local minimum observed at -90° suddenly changes into a local maximum as we enter the uud state. Finally, although the

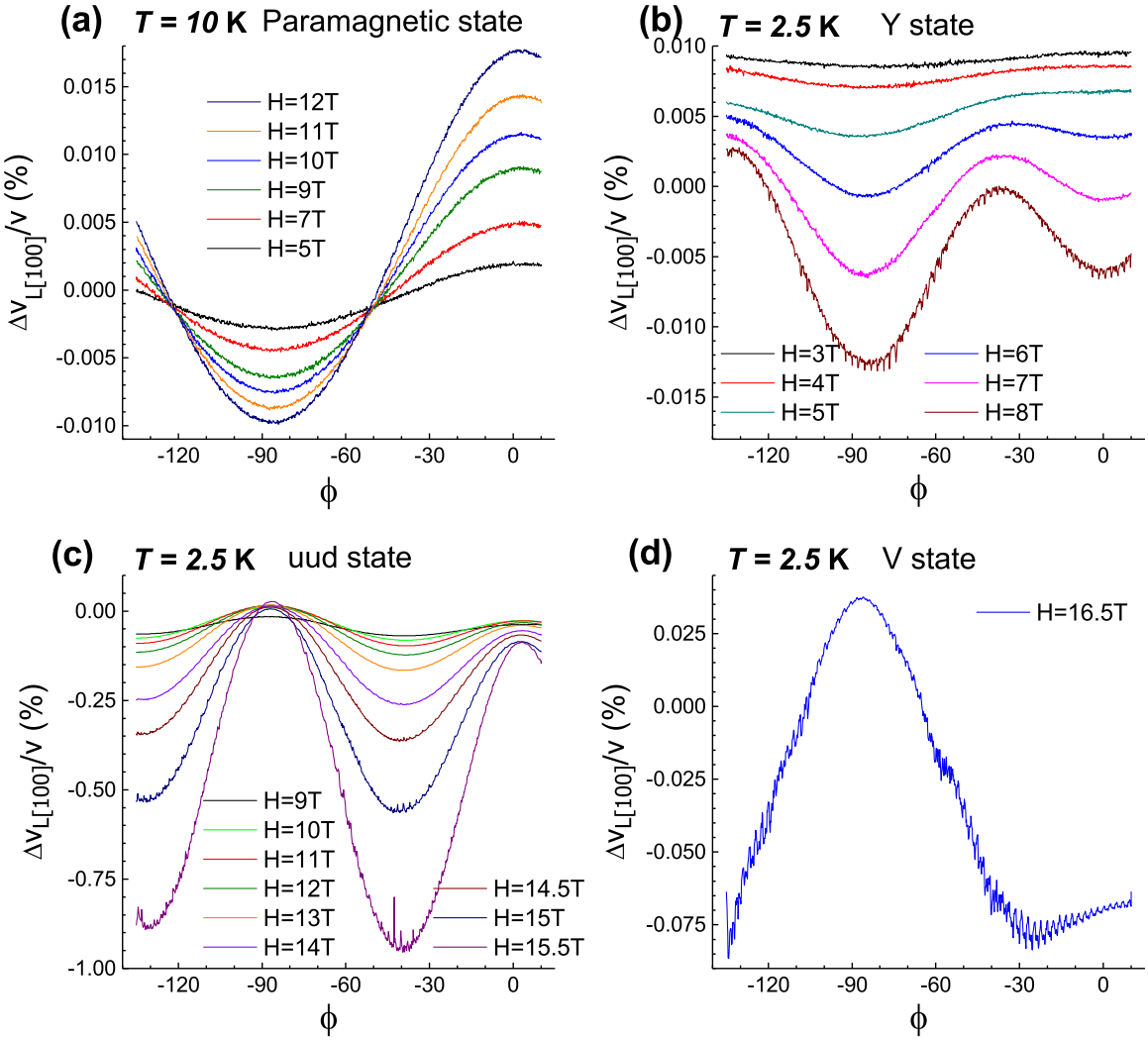

FIG. 3. Field angular (ϕ) dependence of $\Delta v_{L[100]}/v$ for different magnetic field strengths in the basal plane of $Ba_3CoSb_2O_9$, with 0° corresponding to $\mathbf{H} \parallel a$ axis; (a) $T = 10$ K is chosen for paramagnetic state; (b), (c), (d) show results obtained at $T = 2.5$ K in the ordered states (Y, uud, V), respectively.

amplitude of the relative variations generally increases as a function of the field, it suddenly drops by an order of magnitude in the V state ($H_{ab} = 16.5$ T). While the evolution of the angular dependence shown in Fig. 3 is surprisingly complex, we present in Sec. IV a magnetoelestic model which accounts very well for these experimental observations.

IV. MEAN-FIELD MODEL

In order to analyze the experimental data (Fig. 3), a nonlocal Landau free energy approach [30,31] with magnetoelastic couplings is used. This approach is useful as it links the sound velocity directly to the sample magnetization and the antiferromagnetic spin modulations, which are known in general. In that context, the total free energy per unit cell of volume V (at $T = 0$) with nearest-neighbor interaction is written as

$$F = F_s + F_{se} + F_e, \tag{2}$$

$$F_s = \frac{J}{V}\sum_{i\neq j}\mathbf{s}(\mathbf{r}_i)\cdot\mathbf{s}(\mathbf{r}_j) - \frac{g\mu_B}{V}\mathbf{H}\cdot\sum_i \mathbf{s}(\mathbf{r}_i), \tag{3}$$

$$\begin{aligned} F_{se} = &\sum_{i\neq j} K_p(\mathbf{r}_i-\mathbf{r}_j)s(\mathbf{r}_i)\cdot s(\mathbf{r}_j)(e_1+e_2) \\ &+ \sum_{i\neq j} K_m(\mathbf{r}_i-\mathbf{r}_j)\{[s_x(\mathbf{r}_i)s_x(\mathbf{r}_j) \\ &- s_y(\mathbf{r}_i)s_y(\mathbf{r}_j)](e_1-e_2) + 2s_x(\mathbf{r}_i)s_y(\mathbf{r}_j)e_6\}, \end{aligned} \tag{4}$$

$$F_e = \frac{C_{11}^0}{2}(e_1+e_2)^2 + \frac{C_{66}^0}{2}\left(e_6^2 - 4e_1e_2\right). \tag{5}$$

Here, F_s and F_e are the energy associated with the local spin density $\mathbf{s}(\mathbf{r}_i)$ and the elastic energy, while F_{se} represents the linear-quadratic coupling energy (lowest-order coupling invariants) between the strain components e_α (Voigt notation) and $s_\alpha(\mathbf{r}_i)$. Higher-order terms at sixth order that would involve in-plane triangular anisotropy are omitted from the present analysis as they appear to be unnecessary to explain the main features of the experimental results. Due to the quasi-2D character of $Ba_3CoSb_2O_9$ [8] with an easy-plane anisotropy [8], only the energy within the plane which

includes the nearest neighbor exchange energy J, the elastic energy, and the magnetoelastic energy are considered, with the spins being confined to the *ab* plane due to the large exchange anisotropy $J_c/J_1 = 0.026$ [8]. In that case, the 2D invariants depend exclusively on the bare elastic constants C_{11}^0 and C_{66}^0 and two independent magnetoelastic coupling constants $K_{p/m}$. Representing the local spin $\mathbf{s}(\mathbf{r})$ as

$$\mathbf{s}(\mathbf{r}) = \mathbf{m} + \tfrac{1}{2}(\mathbf{S}e^{i\mathbf{Q}\cdot\mathbf{r}} + \mathbf{S}^* e^{-i\mathbf{Q}\cdot\mathbf{r}}), \tag{6}$$

where $\mathbf{m}$ is the magnetization per spin, while the second term represents the antiferromagnetic spin modulation with a wave vector $\mathbf{Q} = (1/3, 1/3, 1)$, as determined experimentally for $Ba_3CoSb_2O_9$ [32]. To account for noncollinear spin configurations, the complex polarization vector $\mathbf{S}$ [in Eq. (6)] is written as

$$\mathbf{S} = \mathbf{S_1} + \mathbf{S_2}, \tag{7}$$

$$\mathbf{S_1} = S(-\cos\beta\cos\theta + i\sin\beta\sin\theta)\,\hat{\mathbf{x}}(\phi), \tag{8}$$

$$\mathbf{S_2} = S(-\cos\beta\sin\theta - i\sin\beta\cos\theta)\,\hat{\mathbf{y}}(\phi), \tag{9}$$

where the angles β and θ take the values ($\beta = \pi/4$, $\theta = 0$) for the 120° state, ($0 < \beta < \pi/4$, $\theta = 0$) in the Y state, ($\beta = 0$, $\theta = 0$) in the uud state, and ($\beta = 0$, $0 < \theta < \pi/2$) in the V state. As the magnetic properties of an equilateral triangular lattice are isotropic, the complex polarization vector $\mathbf{S}$ [Eq. (7)] must be allowed to rotate with the field direction ($\hat{\mathbf{x}}(\phi)$, $\hat{\mathbf{y}}(\phi)$),

$$\hat{\mathbf{x}}(\phi) = \cos\phi\,\hat{\mathbf{x}} + \sin\phi\,\hat{\mathbf{y}}, \tag{10}$$

$$\hat{\mathbf{y}}(\phi) = -\sin\phi\,\hat{\mathbf{x}} + \cos\phi\,\hat{\mathbf{y}}, \tag{11}$$

defined relative to a crystallographic direction imposed by the experimental configuration. For this study, ϕ corresponds to the angle between the field orientation $\mathbf{B}$ and the direction of propagation of the acoustic wave, set to coincide with $\hat{\mathbf{x}}(0) \parallel \mathbf{a}$ axis. Summing over the nearest-neighbor spins, the energy expressed as a function of the dimensionless magnetization $g\,m$ and the antiferromagnetic modulation S reduces to

$$\begin{aligned}
F_s &= -\frac{3JS^2}{4V} + \frac{3Jm^2}{V} - \frac{g\mu_B mH}{V},\\
F_{me} &= K_+^{(m)} g^2 m^2 (e_1 + e_2)\\
&\quad + K_-^{(m)} g^2 m^2 [(e_1 - e_2)\cos 2\phi + e_6 \sin 2\phi],\\
F_{Se} &= K_+^{(S)} S^2 (e_1 + e_2) + K_-^{(S)} S^2 (e_1 - e_2)\cos 2\beta\\
&\quad \times (\cos 2\theta \cos 2\phi - \sin 2\theta \sin 2\phi)\\
&\quad + K_-^{(S)} S^2\, e_6\, \cos 2\beta (\cos 2\phi \sin 2\theta + \cos 2\theta \sin 2\phi).
\end{aligned} \tag{12}$$

The field induced phases are then determined by minimizing F_s with the constrains, $|\mathbf{s}(\mathbf{r}_i)| = 1/2$, imposed by the local spin magnitude. The phase sequence obtained then agrees very well with the experimental phase diagram of $Ba_3CoSb_2O_9$ at low temperatures [18] shown in Fig. 1.

The field angular dependence of the elastic constant $C_{11}(\phi)$ is obtained using [31]

$$C_{11}(\phi) = \frac{\partial^2 F}{\partial e_1^2} - \chi_m \left(\frac{\partial^2 F}{\partial m \partial e_1}\right)^2 - \chi_S \left(\frac{\partial^2 F}{\partial S \partial e_1}\right)^2, \tag{13}$$

where χ_m and χ_S are given by

$$\chi_m = \left(\frac{\partial^2 F}{\partial m^2}\right)^{-1}, \quad \chi_S = \left(\frac{\partial^2 F}{\partial S^2}\right)^{-1}, \tag{14}$$

which represent the uniform magnetic and the antiferromagnetic spin polarization susceptibilities, respectively. For a hexagonal crystal structure, knowing that the velocity of a longitudinal mode propagating along the a axis is given by $v_{L[100]} = \sqrt{C_{11}/\rho}$ [33], where ρ is the mass density, the relative velocity variation as a function of ϕ simplifies to

$$\begin{aligned}
\frac{\Delta v_{L[100]}}{v_{L[100]}} &\simeq \frac{\Delta C_{11}(\phi)}{2C_{11}^0} \simeq \frac{C_{11}(\phi) - C_{11}(0)}{2C_{11}^0},\\
&= A\sin^2(\phi) + B\sin^2(\phi)\cos^2(\phi),
\end{aligned} \tag{15}$$

where, for the Y and plateau states, the angular magnetoelastic coefficients A and B correspond to

$$\begin{aligned}
A &= \frac{8g^4 K_+^{(m)} K_-^{(m)}}{C_{11}^0}\chi_m m^2 + \frac{8K_+^{(S)} K_-^{(S)}}{C_{11}^0}\cos(2\beta)\chi_S S^2,\\
B &= \frac{8g^4 K_-^{(m)2}}{C_{11}^0}\chi_m m^2 + \frac{8K_-^{(S)2}}{C_{11}^0}\cos^2(2\beta)\chi_S S^2.
\end{aligned} \tag{16}$$

Inspection of Eq. (15) immediately reveals that the 180° period is determined by A while B is responsible for a 90° modulation. As shown in Fig. 4, where we present only one experimental curve per magnetic state for clarity, this analytical solution [continuous red lines, Eq. (15)] accounts very well for the observed angular dependence. Thus, all experimental data have been fitted using Eq. (15) in terms of the adjustable parameters A and B. These values are then used to evaluate the magnetoelastic coupling constants $K_\pm^{(m/S)}$ which determine the spin induced lattice distortions (strains) obtained by minimizing Eq. (12) ($\partial F/\partial e_\alpha = 0$), so that

$$\begin{aligned}
e_1 + e_2 &= \frac{K_+^{(m)} m^2 + K_+^{(S)} S^2}{(C_{66}^0 - C_{11}^0)},\\
e_1 - e_2 &= -\frac{K_-^{(m)} m^2 + K_-^{(S)} S^2 \cos(2\beta)}{C_{66}^0}\cos(2\phi),\\
e_6 &= -\frac{K_-^{(m)} m^2 + K_-^{(S)} S^2 \cos(2\beta)}{C_{66}^0}\sin(2\phi).
\end{aligned} \tag{17}$$

Here, the isotropic term $e_1 + e_2$ corresponds to the relative area variation of the basal plane due to the uniform magnetization m and the antiferromagnetic modulation S. However, $e_1 - e_2$ and e_6 correspond to longitudinal and shear distortions leading to a reduction of the crystal symmetry as the magnetic field is rotated away from the direction of propagation of the acoustic wave [$\hat{\mathbf{x}}(\phi = 0) \parallel \mathbf{a}$ axis]. These solutions also indicate that the lattice distortions ($e_1 - e_2$ and e_6) are exclusively related to the magnetoelastic coupling coefficients $K_-^{(m/S)}$. In other words, the magnitude of B provides information

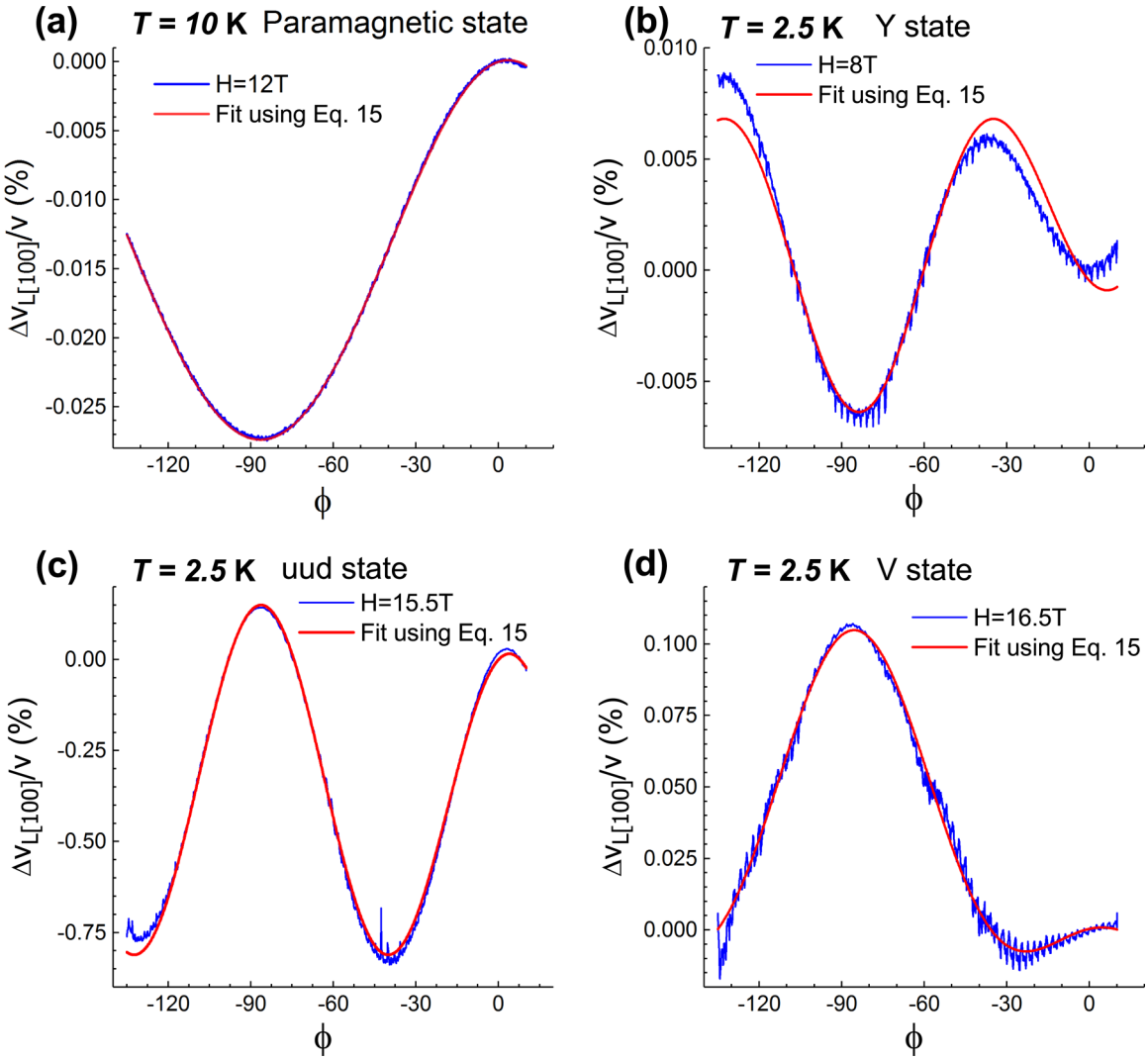

FIG. 4. The red curves illustrate typical fits of $\Delta v_{L[100]}/v$ using Eq. (15) for the data obtained in the paramagnetic state and the different ordered states.

regarding the significance of the spin-induced distortions in triangular lattice antiferromagnets such as $Ba_3CoSb_2O_9$.

V. DATA ANALYSIS

A. Paramagnetic state

First, we analyze the results by fitting the data (using Eq. (15) obtained in the paramagnetic state [Fig. 3(a)]. Considering that for the paramagnetic state the A and B coefficients [Eqs. (16)] depends uniquely on the magnetization, $\mathbf{m} = \chi_m \mathbf{H}$, we present in Fig. 5 the values of A and B as a function of H^2. Using the experimental data presented in Fig. 5, with $\chi_m = 6.5 \times 10^{-2}\ \mu_B/\mathrm{Co}^{2+}$ [11], $C_{11}^0 = (17.3 \pm 0.4) \times 10^{10}\ \mathrm{N/m^2}$, and $C_{66}^0 = (5.3 \pm 0.1) \times 10^{10}\ \mathrm{N/m^2}$ [18], we report in Table I the value of magnetoelastic coupling constants $K_{-/+}^{(m)}$. These values are used to estimate for the field-induced deformations at 3 and 8 T [Eq. (17)]. The magnitude of the deformations reported in Table I for $Ba_3CoSb_2O_9$ are comparable to magnetostriction data obtained for other triangular antiferromagnets such as $CsNiCl_3$ and $RbNiCl_3$ [34].

B. Ordered states

In Fig. 6 we present the evolution of the A and B coefficients determined at 2.5 K in the different magnetically ordered states. These values are compared to results obtained in the paramagnetic state at 10 K (shown as dashed lines in the inset of Fig. 6). The enhanced values of B in the ordered states suggest that the lattice distortions are mainly associated with the antiferromagnetic spin modulation S. Within the framework of the mean-field model presented here [Eq. (16)], considering that there is no microscopic model for χ_S, we simply use that $\chi_S = (\partial^2 F/\partial S^2)^{-1}$ for the evaluation of the magnetoelastic coupling coefficient K_-^S presented in Fig. 7. What is unexpected regarding the field dependence of K_-^S is that its value increases the most in the plateau state and suddenly drops in the V state. This tendency goes against the mean-field numerical predictions as m, S, and β are found to be field independent in the plateau phase. Since all static thermodynamic variables are constant in the plateau state, we can only account for the observed field dependence of K_-^S by considering the possible contribution of spin fluctuations.

TABLE I. Values of magnetoelastic coupling coefficients and magnetostriction effects induced by the magnetic field aligned in the basal plane for $Ba_3CoSb_2O_9$.

$\lvert K_+^{(m)}\rvert$	$(51 \pm 1) \times 10^4$ (N/m^2)		
$\lvert K_-^{(m)}\rvert$	$(5.9 \pm 0.2) \times 10^4$ (N/m^2)		
T		$H = 3$ T	$H = 8$ T
10 K	$\lvert e_1 - e_2\rvert$	$\sim 6.2 \times 10^{-7}$	$\sim 4.4 \times 10^{-6}$
	$\lvert e_1 + e_2\rvert$	$\sim 2.5 \times 10^{-6}$	$\sim 1.7 \times 10^{-5}$

So far we assume that the sound velocity measurements, presented in Fig. 3, are only affected by a mean-field coupling term such as $\langle \mathbf{S}_i \rangle \cdot \langle \mathbf{S}_j \rangle$. However, there exist numerous experimental results that the sound velocity in magnetic systems is also sensitive to spin fluctuations. For example, at the approach of a magnetic state, the velocity generally decreases due to precursor effects associated with spin fluctuations. In that case, the results of K_-^S presented in Fig. 7 could then reflect the field dependence of the spin fluctuations via the dynamic coupling term $\langle \mathbf{S}_i \cdot \mathbf{S}_j \rangle$.

VI. SUMMARY AND CONCLUSIONS

In this work, we determined the strength of the magnetoelastic coupling in the quasi-2D frustrated quantum TLAF $Ba_3CoSb_2O_9$. For that purpose, we developed an experimental approach which does not rely on traditional magnetostriction measurements. It consists of measuring the variation of the sound velocity $v_{L[100]}$ as the magnetic field is rotated in the basal plane at constant temperature. The field angular dependence of the relative velocity variation $\Delta v(\phi)/v$ measured at different fields was then fitted using an analytical solution derived from a Landau model based on symmetry requirements imposed for hexagonal crystal structure. As shown in Fig. 4,

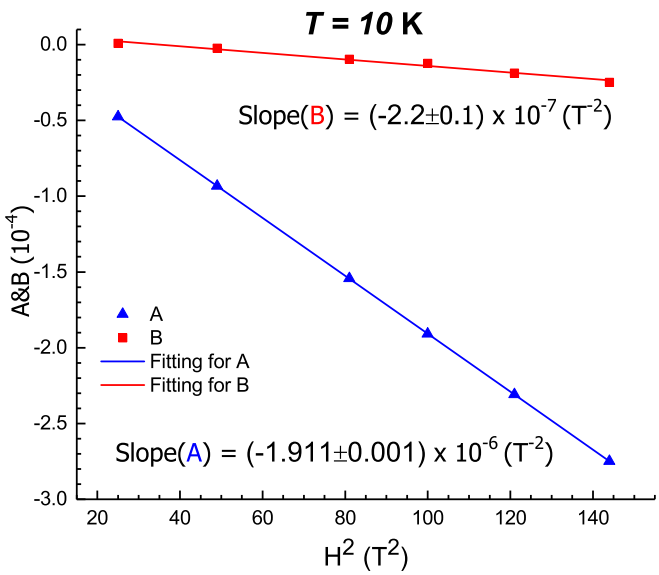

FIG. 5. The blue triangles and red squares represent the field dependence of parameters A and B determined in the paramagnetic phase (10 K) and fitted using Eq. (16) (continuous lines).

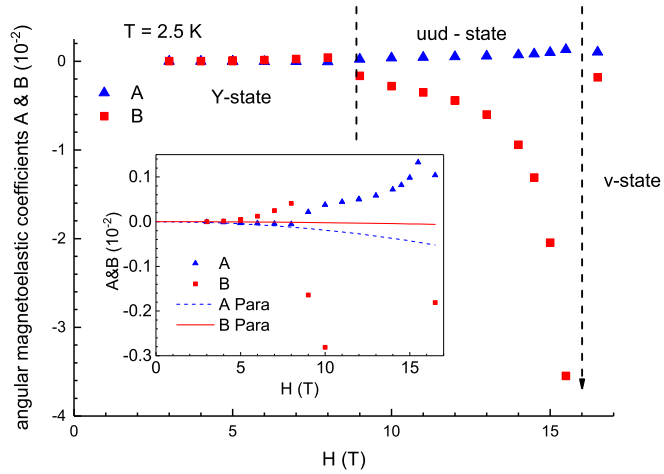

FIG. 6. Angular magnetoelastic coefficients A and B determined at $T = 2.5$ K using Eq. (15). The blue triangles and red squares represent the values of A and B in the different ordered states, which are compared with the values determined in the paramagnetic state (the dashed lines).

the analytical solution [Eq. (15)] accounts very well for the observed angular dependence measured at all temperatures and fields. The adjustable parameters A and B were then used to evaluate the value of magnetoelastic coefficients $K_\pm^{(m/S)}$.

While the observed magnetoelastic coupling in $Ba_3CoSb_2O_9$ is large in comparison to other triangular lattice antiferromagnets, it is still too weak in order to fully account for the observed magnetization plateau width. Based on our numerical analysis, the magnetoelastic mechanism would lead to a plateau width of 0.1 T in comparison with the experimental value of 6 T. We estimate that lattice distortions of the order of $e_1 - e_2 \sim 10^{-3}$ would be required in order to account for the full width of the magnetization plateau in $Ba_3CoSb_2O_9$. To our knowledge, no such large distortions have been observed in $Ba_3CoSb_2O_9$. While we can probably rule out that the magnetization plateau is stabilized by magnetoelastic coupling in the case of $Ba_3CoSb_2O_9$, we attribute the field dependence of the magnetoelastic

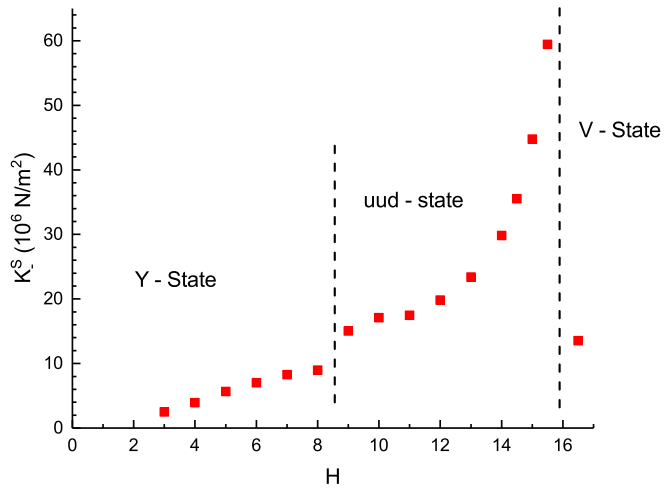

FIG. 7. Field dependence of the magnetoelastic constant K_-^S.

coefficient K_{-}^{S} (Fig. 7) to the effect of spin fluctuations increasing in order to induce and stabilize the magnetization plateau. Another remarkable observation is that our results indicate that these fluctuations are suddenly suppressed or reduced as the V phase is stabilized at higher fields. Thus, to fully account for the experimental results presented in contribution, models including magnetoelastic couplings influenced by spin fluctuations are clearly required. Moreover, as shown by recent experimental work on spin fluctuations on $Ba_3CoSb_2O_9$ [35–37], new theoretical approaches are needed to describe the dynamic magnetic properties of low-dimensional frustrated magnets.

ACKNOWLEDGMENTS

The authors wishes to acknowledge the technical support provided by M. Castonguay. This work was supported by the Natural Sciences and Engineering Research Council of Canada (NSERC) and the Fonds de recherche du Québec, Nature et technologies (FRQNT). Z.L.D. and H.D.Z. acknowledge the support of NSF-DMR- 1350002.

[1] M. F. Collins and O. A. Petrenko, Can. J. Phys. **75**, 605 (1997).
[2] L. Balents, Nature (London) **464**, 199 (2010).
[3] J. Wosnitza, S. A. Zvyagin, and S. Zherlitsyn, Rep. Prog. Phys. **79**, 074504 (2016).
[4] T. Ono, H. Tanaka, H. Aruga Katori, F. Ishikawa, H. Mitamura, and T. Goto, Phys. Rev. B **67**, 104431 (2003).
[5] J. S. White, C. Niedermayer, G. Gasparovic, C. Broholm, J. M. S. Park, A. Y. Shapiro, L. A. Demianets, and M. Kenzelmann, Phys. Rev. B **88**, 060409 (2013).
[6] H. Mitamura, R. Watanuki, K. Kaneko, N. Onozaki, Y. Amou, S. Kittaka, R. Kobayashi, Y. Shimura, I. Yamamoto, K. Suzuki, S. Chi, and T. Sakakibara, Phys. Rev. Lett. **113**, 147202 (2014).
[7] Y. Shirata, H. Tanaka, A. Matsuo, and K. Kindo, Phys. Rev. Lett. **108**, 057205 (2012).
[8] T. Susuki, N. Kurita, T. Tanaka, H. Nojiri, A. Matsuo, K. Kindo, and H. Tanaka, Phys. Rev. Lett. **110**, 267201 (2013).
[9] N. A. Fortune, S. T. Hannahs, Y. Yoshida, T. E. Sherline, T. Ono, H. Tanaka, and Y. Takano, Phys. Rev. Lett. **102**, 257201 (2009).
[10] A. I. Smirnov, H. Yashiro, S. Kimura, M. Hagiwara, Y. Narumi, K. Kindo, A. Kikkawa, K. Katsumata, A. Y. Shapiro, and L. N. Demianets, Phys. Rev. B **75**, 134412 (2007).
[11] A. Sera, Y. Kousaka, J. Akimitsu, M. Sera, T. Kawamata, Y. Koike, and K. Inoue, Phys. Rev. B **94**, 214408 (2016).
[12] M. V. Gvozdikova, P.-E. Melchy, and M. E. Zhitomirsky, J. Phys.: Condens. Matter **23**, 164209 (2011).
[13] T. Sakai and H. Nakano, Phys. Rev. B **83**, 100405 (2011).
[14] G. Koutroulakis, T. Zhou, Y. Kamiya, J. D. Thompson, H. D. Zhou, C. D. Batista, and S. E. Brown, Phys. Rev. B **91**, 024410 (2015).
[15] D. Yamamoto, G. Marmorini, and I. Danshita, J. Phys. Soc. Jpn. **85**, 024706 (2016).
[16] H. Kawamura and S. Miyashita, J. Phys. Soc. Jpn. **54**, 4530 (1985).
[17] H. Kawamura, J. Phys. Soc. Jpn. **53**, 2452 (1984).
[18] G. Quirion, M. Lapointe-Major, M. Poirier, J. A. Quilliam, Z. L. Dun, and H. D. Zhou, Phys. Rev. B **92**, 014414 (2015).
[19] D. Yamamoto, G. Marmorini, and I. Danshita, Phys. Rev. Lett. **114**, 027201 (2015).
[20] M. E. Zhitomirsky, J. Phys. Conf. Ser. **592**, 012110 (2015).
[21] M. T. Heinilä and A. S. Oja, Phys. Rev. B **48**, 7227 (1993).
[22] M. L. Plumer, Phys. Rev. B **44**, 12376 (1991).
[23] F. Wang and A. Vishwanath, Phys. Rev. Lett. **100**, 077201 (2008).
[24] D. L. Bergman, R. Shindou, G. A. Fiete, and L. Balents, Phys. Rev. B **74**, 134409 (2006).
[25] K. Penc, N. Shannon, and H. Shiba, Phys. Rev. Lett. **93**, 197203 (2004).
[26] Y. Doi, Y. Hinatsu, and K. Ohoyama, J. Phys.: Condens. Matter **16**, 8923 (2004).
[27] S. Ya. Istomin, V. A. Koutcenko, E. V. Antipov, F. Lindberg, and G. Svensson, Mater. Res. Bull. **39**, 1013 (2004).
[28] G. Quirion, C. Bidaud, J. A. Quilliam, P. Lejay, V. Simonet, and R. Ballou, Phys. Rev. B **96**, 134433 (2017).
[29] G. Quirion, X. Han, M. L. Plumer, and M. Poirier, Phys. Rev. Lett. **97**, 077202 (2006).
[30] M. L. Plumer and A. Caillé, Phys. Rev. B **37**, 7712 (1988).
[31] G. Quirion, X. Han, and M. L. Plumer, Phys. Rev. B **84**, 014408 (2011).
[32] H. D. Zhou, C. Xu, A. M. Hallas, H. J. Silverstein, C. R. Wiebe, I. Umegaki, J. Q. Yan, T. P. Murphy, J.-H. Park, Y. Qiu, J. R. D. Copley, J. S. Gardner, and Y. Takano, Phys. Rev. Lett. **109**, 267206 (2012).
[33] E. Dieulesaint and D. Royer, *Elastic Waves in Solids* (John Wiley and Sons, New York, 1980).
[34] J. Rayne, J. Collins, and G. White, Solid State Commun. **45**, 681 (1983).
[35] J. Ma, Y. Kamiya, T. Hong, H. B. Cao, G. Ehlers, W. Tian, C. D. Batista, Z. L. Dun, H. D. Zhou, and M. Matsuda, Phys. Rev. Lett. **116**, 087201 (2016).
[36] S. Ito, N. Kurita, H. Tanaka, S. Ohira-Kawamura, K. Nakajima, S. Itoh, K. Kuwahara, and K. Kakurai, Nat. Commun. **8**, 235 (2017).
[37] Y. Kamiya, L. Ge, T. Hong, Y. Qiu, D. L. Quintero-Castro, Z. Lu, H. B. Cao, M. Matsuda, E. S. Choi, C. D. Batista, M. Mourigal, H. D. Zhou, and J. Ma, Nat. Commun. **9**, 2666 (2018).